Letter

Signatures of linear Breit-Wheeler pair production in polarized $\gamma\gamma$ collisions

Qian Zhao,[1] Liang Tang,[2] Feng Wan,[1] Bo-Chao Liu,[1] Ruo-Yu Liu,[3] Rui-Zhi Yang,[4] Jin-Qing Yu,[5,*] Xue-Guang Ren,[1] Zhong-Feng Xu,[1] Yong-Tao Zhao,[1] Yong-Sheng Huang,[6,7,†] and Jian-Xing Li[1,‡]

[1]*Ministry of Education Key Laboratory for Nonequilibrium Synthesis and Modulation of Condensed Matter, Shaanxi Province Key Laboratory of Quantum Information and Quantum Optoelectronic Devices, School of Physics, Xi'an Jiaotong University, Xi'an 710049, China*

[2]*College of Physics and Hebei Key Laboratory of Photophysics Research and Application, Hebei Normal University, Shijiazhuang 050024, China*

[3]*School of Astronomy and Space Science, Nanjing University, 210023 Nanjing, Jiangsu, China*

[4]*CAS Key Labrotory for Research in Galaxies and Cosmology, Department of Astronomy, School of Physical Sciences, University of Science and Technology of China, Hefei, Anhui 230026, China*

[5]*School of Physics and Electronics, Hunan University, Changsha 410082, China*

[6]*School of Science, Shenzhen Campus of Sun Yat-sen University, Shenzhen 518107, China*

[7]*Institute of High Energy Physics, Chinese Academy of Sciences, Beijing 100049, China*

(Received 27 November 2021; accepted 7 April 2022; published 26 April 2022)

The polarization characteristics of the linear Breit-Wheeler (LBW) pair-production process in polarized $\gamma\gamma$ colliders have been investigated via our developed spin-resolved binary collision simulation method. We find that the polarization of γ-photons modifies the kinematics of scattering particles and induces the correlated energy-angle shift of LBW pairs, and the latter's polarization characteristic depends on the helicity configures of scattering particles. We confirm that the polarized $\gamma\gamma$ collider with an asymmetric setup can be performed with currently achievable laser-driven high-density x rays and high-brilliance γ-photon beams to produce abundant polarized LBW pairs, fulfilling the detection power of polarimetries. Our method and results on the polarized LBW process have plenty of significant applications in strong-field physics, high-energy physics and astrophysics, such as calibrating and monitoring the polarized $\gamma\gamma$ collider and challenging the current understanding of astrophysical objects through enhancing the opacity of γ-photons to exacerbate the inconsistency between some observations and standard models.

DOI: 10.1103/PhysRevD.105.L071902

Quantum electrodynamics (QED) predicts the interaction between two real photons, which leads to the linear Breit-Wheeler (LBW) electron-positron ($e^{\pm}$) pair production [1] and photon-photon elastic scattering [2]. Although both the processes are observed in the collision of two virtual photons by means of the equivalent photon approximation of ultrarelativistic heavy-ion beams [3,4], the validation via real photon-photon collisions has never been realized due to the lack of high-brilliance γ-photon beams. One of the most important physical projects in the planned $\gamma\gamma$ collider is to search for higher-order photon-photon scattering, which is solid evidence of the vacuum polarization and is of interest as a search for new physics [5–8]. Because the cross section of the lowest-order LBW process is several orders of magnitude larger than that of the photon-photon scattering [9], it produces useful signatures for diagnostics, feedback, and luminosity optimization in a $\gamma\gamma$ collider [10,11]. Therefore, it is necessary to investigate the comprehensive physics of the LBW process, especially with polarized photons and energy distribution. Moreover, despite the significance in validating basic QED theory, the LBW process is one of the most elemental ingredients of pair plasma production in high-energy astrophysical environment [12], such as γ-ray bursts [13], black hole accretion [14,15], and active galactic nuclei [16].

Thanks to the developments of γ-photon sources driven by the electron beams of laser wakefield acceleration [17], high-brilliance γ-photon beams with MeV energy can be produced experimentally through bremsstrahlung [18,19], nonlinear Thomson scattering [20,21], and inverse Compton scattering [22–24], which open the way to investigate the real photon-photon interaction. Recently, numerous theoretical proposals on the $\gamma\gamma$ collider were put forward to validate the LBW process [9,25–33]. Among those proposals, the $\gamma\gamma$ collider is designed either with

*jinqing.yu@hnu.edu.cn
†huangysh59@mail.sysu.edu.cn
‡jianxing@xjtu.edu.cn

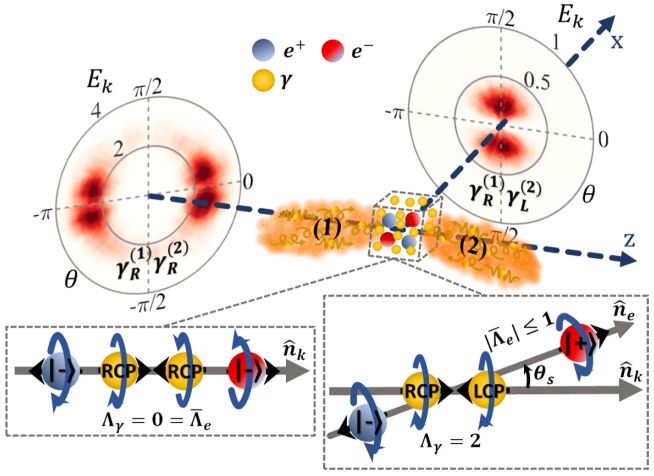

FIG. 1. Scenario of the LBW pair production in a colliding setup of polarized γ-photon beams in x-z plane in the laboratory frame. The pair spectra are presented in the plane of polar angle θ and kinematic energy E_k. The lower sketches show the helicity transfer of the LBW process in the center of mass frame, and Λ_γ is the total helicity of two-photon system in the direction of photon momentum $\hat{n}_k$. The scattered pair carries the mean total helicity $\bar{\Lambda}_e$ in the direction of electron momentum $\hat{n}_e$, $|\pm\rangle$ represent the positive and negative helicity states, corresponding to the right-hand and left-hand spirals, respectively, and $\gamma_{R/L}^{(1)/(2)}$ denote right-hand circular polarization (RCP) or left-hand circular polarization (LCP) photon in beam (1) and beam (2), respectively.

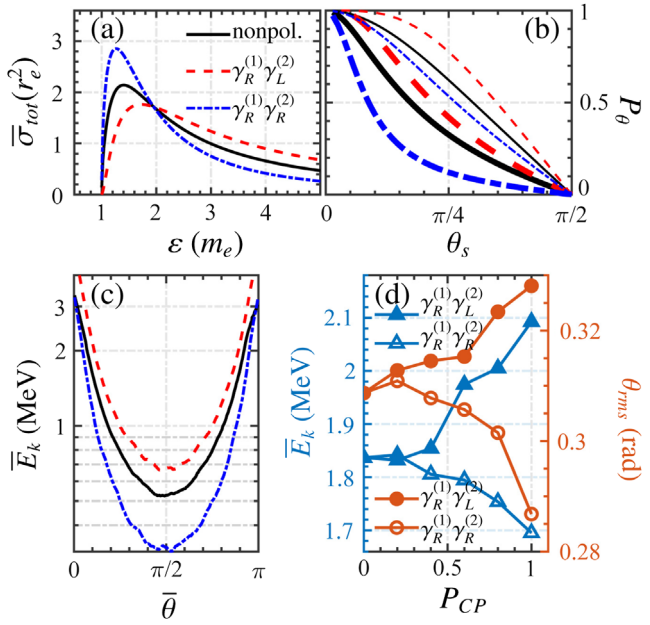

FIG. 2. (a) $\bar{\sigma}_{\rm tot}$ vs the c.m. energy ε for different collision schemes. The black-solid, red-dashed, and blue-dash-dotted lines in (a) and (b) indicate the cases of employing non-polarized, $\gamma_R^{(1)}\gamma_L^{(2)}$ and $\gamma_R^{(1)}\gamma_R^{(2)}$ γ-photons, respectively. (b) $P_\theta = \bar{\sigma}_\theta/\bar{\sigma}_{\rm tot}$ vs θ_s. The thin and thick lines correspond to $\varepsilon = 1.4$ and 4, respectively. (c) Average kinetic energy $\bar{E}_k$ vs average polar angle $\bar{\theta}$ of positrons. (d) $\bar{E}_k$ and divergence angle θ_{rms} (root-mean-square deviation) of positrons beamed into $0 < \theta < \pi/6$ vs average circular polarization P_{CP} of the initial γ-photon beam. The results in (c) and (d) are simulated with colliding γ-photon beams with an exponential energy distribution at an average energy 2 MeV and a divergence angle 0.1 rad in the laboratory frame.

GeV-energy photons from bremsstrahlung inside a high-Z target and keV-energy partner photon from laser-target radiation or x-ray free electron laser [25,31,33], or with two same MeV γ-photon sources from a laser-driven synchrotron or nonlinear Compton scattering [9,26–28,30]. Moreover, the dominated LBW process is studied in laser-driven plasmas [34,35], and the quasiparticle-hole pair production in gapped graphene monolayers can be analogous to the LBW process [36]. However, the above proposals mainly focus attention on the large pair yield, but generally ignore the inherent spin effects of scattering particles. The polarization transfer (i.e., helicity transfer) between initial photons and final $e^\pm$ pairs is associated with their spin angular momentum. Based on the production of high-brilliance photons with highly-circular polarization [37–42], the LBW process can be investigated in a polarized $\gamma\gamma$ collider. The fundamental physics of helicity in the LBW process has been analyzed qualitatively from the perspective of angular momentum conservation [43]. The latest experiment confirms that the linearly-polarized photons can induce the azimuthal-angle distribution of the LBW pairs [4], since the linear polarization is related to the azimuthal angle of pair momenta. In addition, the impact of energy distribution of γ-photon beam on the LBW pair yield is analyzed in a semianalytical model [32]. However, considering realistic polarization and energy distribution into laser-driven γ-photon beams, the spin-associated momentum and polarization characteristics of the LBW process have not been uncovered and are still great challenges.

In this paper, we investigate the complete polarization effects in the LBW process by virtue of our newly developed spin-resolved Monte Carlo (MC) simulation method, which is applicable for general binary collisions of leptons and photons (see the interaction scenario in Fig. 1). We find that the circular polarization of γ-photons can modify the kinematics of scattering particles and induces a correlated energy-angle shift of the LBW pairs [see Fig. 1 (top) and more details in Fig. 2], and the polarization characteristic of the LBW pairs depends on the helicity configures of scattering particles [see Fig. 1 (bottom) and more details in Fig. 3]. Our method confirms that the polarized $\gamma\gamma$ collider with an asymmetric setup can be performed with currently achievable laser facilities (see Table I), and the considered polarization effects may have significant applications in high-energy astrophysics.

Let us first summarize our simulation method for calculating the production and polarization of the LBW pairs. Employing the standard treatment of particle density

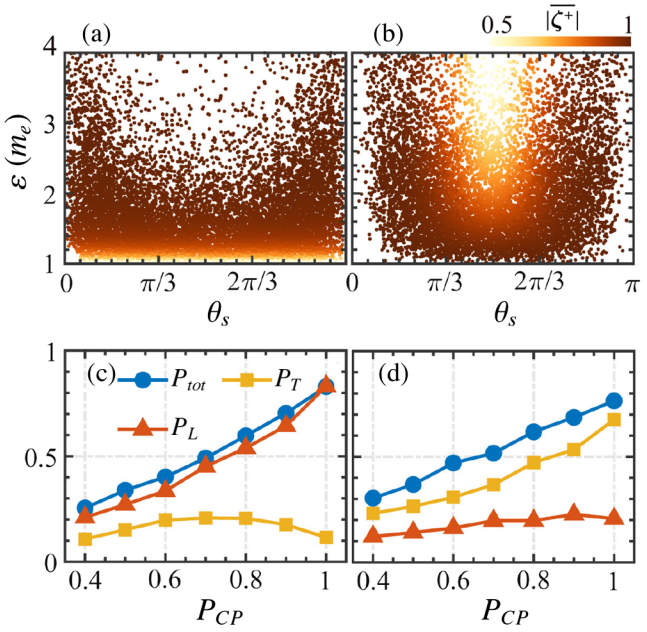

FIG. 3. (a) and (b): Distributions of $|\overline{\boldsymbol{\zeta}^+}|$ of produced positrons for the $\gamma_R^{(1)}\gamma_R^{(2)}$ and $\gamma_R^{(1)}\gamma_L^{(2)}$ collisions, respectively. (c) and (d): Variations of $P_{\rm tot}$, P_L, and P_T of positrons with respect to P_{CP} of the γ-photon beam, extracted from positrons within $0 < \theta < \pi/6$ for the $\gamma_R^{(1)}\gamma_R^{(2)}$ collision and $\pi/3 < \theta < 2\pi/3$ for the $\gamma_R^{(1)}\gamma_L^{(2)}$ collision, respectively. Here employed γ-photon beams both have an uniform energy distribution between 0.1 MeV–2 MeV.

matrixes in the scattering amplitude of incoherent binary collisions [43–48], the polarized LBW cross section in center of mass (c.m.) frame is obtained as

$$\frac{\mathrm{d}\sigma}{\mathrm{d}\Omega} = \sigma_0\left[F + \sum_{i=1}^{3}(G_i^+\zeta_i^+ + G_i^-\zeta_i^-) + \sum_{i,j=1}^{3} H_{i,j}\zeta_i^+\zeta_j^-\right], \quad (1)$$

where $\sigma_0 = r_e^2 m_e^2|\boldsymbol{p}_e|/16\varepsilon^3$, Ω is the solid angle, $\boldsymbol{p}_e$ the c.m. momentum of electron, ε the c.m. energy of photon, electron and positron (they are equal in the c.m. frame), m_e and r_e the electron mass and classical radius, respectively, $\zeta_i^\pm$ the spin components of electron ("−") and positron ("+"), and the factors F, $G_i^\pm$, and $H_{i,j}$ include the photon Stokes parameters ξ_i [44] and are given in [49]. Summing over $\zeta_i^\pm$ and integrating over Ω, one obtains

$$\bar{\sigma}_{\rm tot} = \frac{r_e^2 m_e^4 \pi}{4\varepsilon^4}\sqrt{\frac{\tilde{s}-4}{\tilde{s}}}\Big(-\tilde{s} - 4 + 2\xi_1^{(1)}\xi_1^{(2)} + 3\tilde{s}\xi_2^{(1)}\xi_2^{(2)} - 2\xi_3^{(1)}\xi_3^{(2)}\Big) + \frac{16\pi}{\tilde{s}}\tanh^{-1}\sqrt{\frac{\tilde{s}-4}{\tilde{s}}}\Big(2\tilde{s}^2 + 8\tilde{s} - 16 + 8\xi_1^{(1)}\xi_1^{(2)} - 2\tilde{s}^2\xi_2^{(1)}\xi_2^{(2)} - 8\xi_3^{(1)}\xi_3^{(2)}\Big), \quad (2)$$

TABLE I. Average current I and polarization (Pol.) of produced positrons (electrons) extracted from the polar angle range of $\Delta\theta$. The symmetric setup includes photons number N_γ, brilliance $\mathcal{B}_\gamma$(photons s^{-1} mm^{-2} mrad^{-2} 0.1% BW), and cross angle of colliding γ-photon beams. And the asymmetric setup considers a RCP γ-photon beam with 80% polarization colliding with a x-ray beam with uniform density n_X. Employed γ-photon beam in the symmetric (asymmetric) setup has a ∼80 fs duration and an exponential energy distribution with an average energy of 2 (100) MeV.

Beam parameters	Collisions	I [mA]	Pol.	$\Delta\theta$ [rad]
Symmetric Setup: N_γ: 1×10^{11} Phots.	$\gamma_R^{(1)}\gamma_R^{(2)}$	4.231	P_L	$0\pm\pi/6$
$\mathcal{B}_\gamma$: 1.5×10^{23} Cross-angle: 5°	$\gamma_R^{(1)}\gamma_L^{(2)}$	3.952	P_T	$\pi/2\pm\pi/6$
Asymmetric Setup: N_γ: 1×10^{7} Phots.	$\gamma_R^{(1)}(0.8)$	1.052	$P_L(0.348)$,	0 ± 0.02
$\mathcal{B}_\gamma$: 2.2×10^{21}	x ray		$P_T(0.151)$	
n_X: 9.3×10^{23} cm^{-3}				

where $\tilde{s} = 4\varepsilon^2/m_e^2$. Relativistic units with $c = \hbar = 1$ are used throughout.

In our considered collision scenario, a γ-photon beam is initialized with a specific energy distribution and divergence angle in laboratory frame. During the beam-beam collision, the colliding region is meshed into solid cells at every time step, and the probable colliding photons inside a cell are sampled by the Thomson cross section and paired by no-time-count method [50], as illustrated in Fig. 1 (top). By the Lorentz boost along the c.m. frame velocity $\boldsymbol{\beta}_{cm}$ [51–53], every set of paired photons with $\tilde{s} > 4$ are permitted for the single BW process in Eq. (1) by using the acceptance-rejection method. For each BW event, the c.m. momentum $\boldsymbol{p}_e$ is determined in the defined momentum configure (see Fig. 1 in [49]) where the scattering angle θ_s is defined as the angle between $\boldsymbol{p}_e$ and $\boldsymbol{k}$. Here θ_s is calculated by solving $\bar{\sigma}_\theta/\bar{\sigma}_{\rm tot} = R_1 \in (-1, 1)$, where R_1 is an uniform random number and $\bar{\sigma}_\theta = \sqrt{\tilde{s}(\tilde{s}-4)/4}\int_{-|\cos\theta_s|}^{|\cos\theta_s|}\mathrm{d}\bar{\sigma}$. Moreover, the energy and momenta of $e^\pm$ in the laboratory frame are obtained by the inverse Lorentz boost acting on ε and $\boldsymbol{p}_e$.

The mean spin polarization vectors of electron and positron $\overline{\boldsymbol{\zeta}^\pm}$ are determined by the defined three-vector basis [45,49] and their components can be analytically calculated via $\overline{\zeta^\pm}_i = G_i^\pm/F$ [44]. With the determined $\boldsymbol{p}_e$, the mean helicities of a pair are expressed as $\lambda_\pm = \mp\,\overline{\boldsymbol{\zeta}^\pm}\boldsymbol{p}_e/2|\boldsymbol{p}_e|$, and the corresponding helicity configure is illustrated in Fig. 1 (bottom). In our MC method, the projections of $\overline{\boldsymbol{\zeta}^\pm}$ onto the defined spin states $\boldsymbol{D}^\pm$ (unit vectors) of a detector are calculated with transition probabilities, and the latter determine the sign of components $D_i^\pm = \overline{\zeta^\pm}_i/|\overline{\boldsymbol{\zeta}^\pm}|$. Consequently, the total beam polarization

is calculated by $P_{\rm tot}=\sqrt{(\overline{D_1^{\pm}})^2+(\overline{D_2^{\pm}})^2+(\overline{D_3^{\pm}})^2}$ with the averaged components $\overline{D_i^{\pm}}$ over the particle number [54]. Aligning $\boldsymbol{D}^{\pm}$ to the parallel or perpendicular direction of the momenta can further obtain the longitudinal polarization P_L or transverse polarization P_T for $e^{\pm}$ beams. (More details of our simulation method are clarified in the Supplemental Material [49].)

Impact of the γ-photon polarization on the energy and polar angle distributions of the LBW pairs is shown in Fig. 2. $\bar{\sigma}_{\rm tot}$ of the $\gamma_R^{(1)}\gamma_R^{(2)}$ case increases about 33% at the peak energy and narrows the spectrum, compared with that of the nonpolarized case [see Fig. 2(a)], while the linear polarization only modifies the amplitude because it has no impact on θ_s [49]. A definite shaped $P_\theta(\theta_s)$ implies that the produced electron (positron) is scattered into a certain range of $\mathrm{d}\theta_s$ with a corresponding probability of $\mathrm{d}P_\theta$ [see Fig. 2(b)]. The reactions within $\theta_s \lesssim \pi/6$ in the $\gamma_R^{(1)}\gamma_L^{(2)}$ collision near the threshold energy are almost forbidden due to the approximate zero probabilities. By contrast, the dominated reactions occur within $\theta_s \lesssim \pi/6$ in the $\gamma_R^{(1)}\gamma_R^{(2)}$ collision at the energy far beyond the threshold. Therefore, the distinct energy-angle spectra can be produced by the quasimonoenergetic beams in two collision schemes, and the $\gamma_R^{(1)}\gamma_L^{(2)}$ ($\gamma_R^{(1)}\gamma_R^{(2)}$) collision with a Gaussian energy spectrum, an average energy of 0.6 (1.8) MeV and a 30% energy spread produces the dipole (quadrupole) angular spectrum, which distributes perpendicular to (parallel with) the z-axis, as shown in Fig. 1 (top). The distinct energy-correlated θ_s in these two interaction schemes causes the energy-angle correlation of the pairs, whereby the $\gamma_R^{(1)}\gamma_L^{(2)}$ collision results in the larger kinetic energy $\bar{E}_k$ than that of the $\gamma_R^{(1)}\gamma_R^{(2)}$ collision [see Fig. 2(c)]. As the initial circular polarization (P_{CP}) of γ-photons increases, in the $\gamma_R^{(1)}\gamma_L^{(2)}$ collision the average kinetic energy $\bar{E}_k$ and the divergence angle θ_{rms} of positrons both increase as well, while in the $\gamma_R^{(1)}\gamma_R^{(2)}$ collision the tendency is inverse [see Fig. 2(d)]. Thus, θ_{rms} is positively correlated to $\bar{E}_k$. The influence of the energy and divergence-angle fluctuations of the γ-photon beams on θ_{rms} and $\bar{E}_k$ is estimated, and the results indicate that the polarization-induced signatures of the energy-angle shift can be resolved as the fluctuations of the divergence angle and the average energy are less than 50% and 5%, respectively (see [49]). Note that the correlated polar angle and energy distributions of the LBW pairs can be resolved precisely in experiments by the single particle detector [33].

Particularly, the spin-polarization of the LBW pairs is derived from the circular polarization of parent γ-photons. For the $\gamma_R^{(1)}\gamma_R^{(2)}$ collision, the partial polarization is produced near the threshold energy of the pair production [see Fig. 3(a)], while for the $\gamma_R^{(1)}\gamma_L^{(2)}$ collision, the partial polarization is produced around $\theta_s=\pi/2$ [see Fig. 3(b)]. It is nontrivial to reveal the variation of the positron polarization with respect to the γ-photon polarization. For the $\gamma_R^{(1)}\gamma_R^{(2)}$ collision, P_L dominates the polarization and increases linearly, and P_T [attributed to the $\mathrm{d}\sigma_{+-\pm\mp}$ channel; see Fig. 4(e)] is less than 0.2 as P_{CP} varies [see Fig. 3(c)], since the produced pairs possess sole negative helicities [see Fig. 4(a)]. While, for the $\gamma_R^{(1)}\gamma_L^{(2)}$ collision P_T dominates the polarization [see Fig. 3(d)], since the produced pairs possess the mixed helicity states [55] around $\theta_s=\pi/2$ and the magnitude of P_T is affected by the extracted polar angle range [see Fig. 4(b)]. Thus, one could observe the signatures of polarization in the LBW process either via detecting P_L in the $\gamma_R^{(1)}\gamma_R^{(2)}$ collision around the colliding axis or via detecting P_T in the $\gamma_R^{(1)}\gamma_L^{(2)}$ collision around the perpendicular direction of the colliding axis.

The physical mechanism of the helicity transfer in the LBW process is analyzed in Fig. 4. The polarization is derived from the mean helicity distribution, and the $\gamma_R^{(1)}\gamma_R^{(2)}$

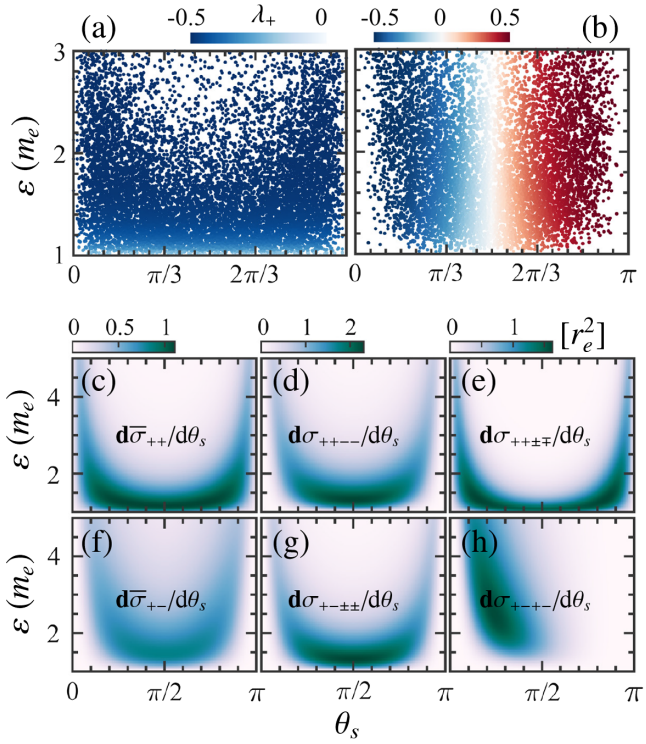

FIG. 4. (a) and (b): Distributions of the positron helicity λ_+ with respect to θ_s and ε in the c.m. frame for the $\gamma_R^{(1)}\gamma_R^{(2)}$ and $\gamma_R^{(1)}\gamma_L^{(2)}$ collisions, respectively. Employed parameters are the same with those in Fig. 3. (c)–(e) [(f)–(h)]; Differential cross sections for different helicity channels for the $\gamma_R^{(1)}\gamma_R^{(2)}$ ($\gamma_R^{(1)}\gamma_L^{(2)}$) collision. Here the subscripts from the first to the fourth in sequence denote positive ("+") or negative ("−") helicity eigenstates of $\gamma^{(1)}$, $\gamma^{(2)}$, e^-, and e^+, and $\mathrm{d}\bar{\sigma}$ indicates the spin-summarized cross section and is calculated via $\sigma_0 F$ in Eq. (1).

collision leads to the energy-dependent negative helicities, while the $\gamma_R^{(1)}\gamma_L^{(2)}$ collision leads to the angle-dependent alternating helicities (vary between −0.5 and 0.5) [see Figs. 4(a) and (b)]. The positron helicity originates from the superposition of various helicity eigenstates with different weights determined by the differential cross section. There are only three nonvanished helicity channels $d\sigma_{++--}$, $d\sigma_{+++-}$, and $d\sigma_{++-+}$ for the $\gamma_R^{(1)}\gamma_R^{(2)}$ collision [see Figs. 4(d) and 4(e)]. Here, $d\sigma_{++\pm\mp}$ dominate the reaction near the threshold energy, produce the positrons at the helicity states $|+\rangle$ or $|-\rangle$ with the same weights, and consequently, cancel each other (i.e., P_L vanishes and P_T maximizes). Thus, only the channel of $d\sigma_{++--}$ contributes to the state $|-\rangle$, i.e., $d\sigma_{++--}$ solely induces P_L. These helicity channels finally result in the mean helicity distribution in Fig. 4(a) and the corresponding positron polarization in Fig. 3(a). Similarly, in the $\gamma_R^{(1)}\gamma_L^{(2)}$ collision, there are four helicity channels $d\sigma_{+-\pm\pm}$ and $d\sigma_{+-\pm\mp}$ (note that here $d\sigma_{+--+}$ is symmetric about $\theta_s = \pi/2$ with $d\sigma_{+-+-}$ and thus is not shown) [see Figs. 4(g) and (h)]. $d\sigma_{+-\pm\pm}$ only contribute to P_T and $d\sigma_{+-\pm\mp}$ mainly to P_L [see Figs. 4(b) and 3(b)].

For the experimental feasibility, the symmetric and asymmetric setups are considered to design the polarized $\gamma\gamma$ collider, as shown in Table I. The symmetric setup reveals the polarization-associated signatures in both of momentum and spin (see Figs. 2 and 3), and the required minimal brilliance of the γ-photon beam is rather high in order to produce a resolvable mA current for the polarimetry. In the asymmetric setup, the RCP γ-photon beam injects into a nonpolarized x-ray bath with an uniform energy distribution between 1 keV–3 keV and an isotropic angular distribution, produce a strongly collimated positron (electron) beam with moderate P_L and P_T. Because the asymmetric setup utilizes the dense x-ray bath generated by laser-heated hohlraum [25] or laser-irradiated target [33], it can significantly reduce the required minimal brilliance of the γ-photon beam as the density of x-rays reaches above 10^{20} cm^{-3}. The experimentally feasible γ-photon sources with brilliance $\sim 10^{22}$ can be generated through the Compton scattering [22,56], and the polarized one is also available by the bremsstrahlung radiation with a photon number of $\sim 10^8$ [25,40]. Furthermore, the stabilities of the pair yield and polarization in the asymmetric setup are estimated by varying the divergence angle and polarization of the γ-photon beam, the results (see [49]) indicate that both the variations of the initial polarization and divergence angle have slight influence on the current of produced electrons (positrons), and the longitudinal polarization can reach the maximum 50% as the divergence and polarization of γ-photon beam increase. In terms of the polarization detection, the $e^{\pm}$ polarimetry technology has achieved a high precision $\lesssim 1\%$, e.g., Compton transmission polarimetry [38–40] and Mott polarimetry [57–59], which are both applicable at the energy of 0.1 MeV–10 MeV and can response the current as low as $\lesssim 100$ μA [57,58].

Furthermore, we underline that the LBW process is also widely involved in high-energy astrophysical phenonema. The measured γ-ray spectra of those intense compact astrophysical objects (such as GRBs, blazars, pulsar, and etc) are supposed to be attenuated at the high-energy end by the low-energy radiation therein via this process [60–65]. Both the low-energy radiation and the γ-ray radiation, which generally arise from the synchrotron radiation and the inverse Compton scattering respectively, can be polarized in the presence of magnetic field. Taking into account the polarized LBW process would enhance the opacity of γ-photons of those sources and consequently exacerbate the inconsistency between some observations and standard models, which may challenge the current understanding on the astrophysical objects.

In conclusion, we develop a fully spin-resolved simulation method for general binary collisions to investigate the complete polarization effects of the LBW process in polarized $\gamma\gamma$ collision. Qualitative signatures of polarized LBW process are imprinted on momentum and spin of produced pairs. Our results of polarized LBW processes are effective in calibrating and monitor the upcoming polarized $\gamma\gamma$ collider, and pave the way for proceeding the elusive photon-photon scattering. Moreover, the polarization-induced fluctuations of the $e^{\pm}$ density in high-energy astrophysical objects possibly associate with certain of significant observations, which calls for the further investigation.

This work is supported by the National Natural Science Foundation of China (Grants No. 12022506, No. 11874295, No. 11875219, No. 11905169 and No. 12175058), the China Postdoctoral Science Foundation (Grant No. 2020M683447), the Open Fund of the State Key Laboratory of High Field Laser Physics (Shanghai Institute of Optics and Fine Mechanics, the Natural Science Foundation of Hunan Province, China (Grant No. 2020JJ5031), the project of Science and Technology on plasma physics Laboratory (Grant No. 6142A04190111), the Innovation Project of IHEP (Grants No. 542017IHEPZZBS11820 and No. 542018IHEPZZBS12427), and the CAS Center for Excellence in Particle Physics (CCEPP).

[1] G. Breit and J. A. Wheeler, Collision of two light quanta, Phys. Rev. **46**, 1087 (1934).

[2] O. Halpern, Scattering processes produced by electrons in negative energy states, Phys. Rev. **44**, 855 (1933).

[3] ATLAS Collaboration, Evidence for light-by-light scattering in heavy-ion collisions with the ATLAS detector at the LHC, Nat. Phys. **13**, 852 (2017).

[4] J. Adam, L. Adamczyk, J. Adams, J. Adkins, G. Agakishiev, M. M. Aggarwal, Z. Ahammed, I. Alekseev, D. Anderson, A. Aparin *et al.* (STAR Collaboration), Measurement of e^+e^- Momentum and Angular Distributions from Linearly Polarized Photon Collisions, Phys. Rev. Lett. **127**, 052302 (2021).

[5] T. Yamaji, T. Inada, T. Yamazaki, T. Namba, S. Asai, T. Kobayashi, K. Tamasaku, Y. Tanaka, Y. Inubushi, K. Sawada, M. Yabashi, and T. Ishikawa, An experiment of X-ray photon-photon elastic scattering with a Laue-case beam collider, Phys. Lett. B **763**, 454 (2016).

[6] I. Drebot, A. Bacci, D. Micieli, E. Milotti, V. Petrillo, M. R. Conti, A. R. Rossi, E. Tassi, and L. Serafini, Study of photon–photon scattering events, Nucl. Instrum. Methods Phys. Res., Sect. A **865**, 9 (2017).

[7] T. Takahashi, G. An, Y. Chen, W. Chou, Y. Huang, W. Liu, W. Lu, J. Lv, G. Pei, S. Pei, C. P. Shen, B. Sun, C. Zhang, and C. Zhang, Light-by-Light scattering in a photon-photon collider, Eur. Phys. J. C **78**, 893 (2018).

[8] M. Sangal, C. H. Keitel, and M. Tamburini, Observing light-by-light scattering in vacuum with an asymmetric photon collider, Phys. Rev. D **104**, L111101 (2021).

[9] I. Drebot, D. Micieli, E. Milotti, V. Petrillo, E. Tassi, and L. Serafini, Matter from light-light scattering via Breit-Wheeler events produced by two interacting Compton sources, Phys. Rev. Accel. Beams **20**, 043402 (2017).

[10] A. V. Pak, D. V. Pavluchenko, S. S. Petrosyan, V. G. Serbo, and V. I. Telnov, Measurement of $\gamma\gamma$ and γe luminosities and polarizations at photon colliders, Nucl. Phys. B, Proc. Suppl. **126**, 379 (2004).

[11] J. Esberg, U. I. Uggerhøj, B. Dalena, and D. Schulte, Strong field processes in beam-beam interactions at the compact linear collider, Phys. Rev. ST Accel. Beams **17**, 051003 (2014).

[12] R. Ruffini, G. Vereshchagin, and S. Xue, Electronpositron pairs in physics and astrophysics: From heavy nuclei to black holes, Phys. Rep. **487**, 1 (2010).

[13] P. Kumar and B. Zhang, The physics of gamma-ray bursts relativistic jets, Phys. Rep. **561**, 1 (2015).

[14] K. Hirotani and H. Y. Pu, Energetic gamma radiation from rapidly rotating black holes, Astrophys. J. **818**, 50 (2016).

[15] K. Akiyama, A. Alberdi, W. Alef, K. Asada, R. Azulay, A. K. Baczko, D. Ball, M. Baloković, J. Barrett, D. Bintley *et al.*, First M87 event horizon telescope results. v. physical origin of the asymmetric ring, Astrophys. J. Lett. **875**, L5 (2019).

[16] M. Böttcher, Progress in multi-wavelength and multi-messenger observations of blazars and theoretical challenges, Galaxies **7**, 20 (2019).

[17] E. Esarey, C. B. Schroeder, and W. P. Leemans, Physics of laser-driven plasma-based electron accelerators, Rev. Mod. Phys. **81**, 1229 (2009).

[18] Y. Glinec, J. Faure, L. LeDain, S. Darbon, T. Hosokai, J. J. Santos, E. Lefebvre, J. P. Rousseau, F. Burgy, B. Mercier, and V. Malka, High-Resolution γ-ray Radiography Produced by a Laser-Plasma Driven Electron Source, Phys. Rev. Lett. **94**, 025003 (2005).

[19] N. Lemos, F. Albert, J. L. Shaw, D. Papp, R. Polanek, P. King, A. L. Milder, K. A. Marsh, A. Pak, B. B. Pollock *et al.*, Bremsstrahlung hard X-ray source driven by an electron beam from a self-modulated laser wakefield accelerator, Plasma Phys. Control. Fusion **60**, 054008 (2018).

[20] G. Sarri, D. J. Corvan, W. Schumaker, J. M. Cole, A. Di Piazza, H. Ahmed, C. Harvey, C. H. Keitel, K. Krushelnick, S. P. D. Mangles, Z. Najmudin, D. Symes, A. G. R. Thomas, M. Yeung, Z. Zhao, and M. Zepf, Ultrahigh Brilliance Multi-MeV γ-ray Beams from Nonlinear Relativistic Thomson Scattering, Phys. Rev. Lett. **113**, 224801 (2014).

[21] W. Yan, C. Fruhling, G. Golovin, D. Haden, J. Luo, P. Zhang, B. Zhao, J. Zhang, C. Liu, M. Chen, S. Chen, S. Banerjee, and D. Umstadter, High-order multiphoton thomson scattering, Nat. Photonics **11**, 514 (2017).

[22] C. Yu, R. Qi, W. Wang, J. Liu, W. Li, C. Wang, Z. Zhang, J. Liu, Z. Qin, M. Fang *et al.*, Ultrahigh brilliance quasi-monochromatic MeV gamma-rays based on self-synchronized all-optical compton scattering, Sci. Rep. **6**, 29518 (2016).

[23] J. M. Cole *et al.*, Experimental Evidence of Radiation Reaction in the Collision of a High-Intensity Laser Pulse with a Laser-Wakefield Accelerated Electron Beam, Phys. Rev. X **8**, 011020 (2018).

[24] X. L. Zhu, M. Chen, S. M. Weng, T. P. Yu, W. M. Wang, F. He, Z. M. Sheng, P. McKenna, D. A. Jaroszynski, and J. Zhang, Extremely brilliant GeV γ-rays from a two-stage laser-plasma accelerator, Sci. Adv. **6**, eaaz7240 (2020).

[25] O. J. Pike, F. Mackenroth, E. G. Hill, and S. J. Rose, A photon-photon collider in a vacuum hohlraum, Nat. Photonics **8**, 434 (2014).

[26] X. Ribeyre, E. d'Humieres, O. Jansen, S. Jequier, V. T. Tikhonchuk, and M. Lobet, Pair creation in collision of gamma-ray beams produced with high-intensity lasers, Phys. Rev. E **93**, 013201 (2016).

[27] O. Jansen, T. Wang, D. J. Stark, E. dHumires, T. Toncian, and A. V. Arefiev, Leveraging extreme laser-driven magnetic fields for gamma-ray generation and pair production, Plasma Phys. Control. Fusion **60**, 054006 (2018).

[28] J. Q. Yu, H. Y. Lu, T. Takahashi, R. H. Hu, Z. Gong, W. J. Ma, Y. S. Huang, C. E. Chen, and X. Q. Yan, Creation of Electron-Positron Pairs in Photon-Photon Collisions Driven by 10-PW Laser Pulses, Phys. Rev. Lett. **122**, 014802 (2019).

[29] T. Wang and A. Arefiev, Comment on "Creation of Electron-Positron Pairs in Photon-Photon Collisions Driven by 10-PW Laser Pulses", Phys. Rev. Lett. **125**, 079501 (2020).

[30] T. Wang, X. Ribeyre, Z. Gong, O. Jansen, E. d'Humières, D. Stutman, T. Toncian, and A. Arefiev, Power Scaling for Collimated γ-ray Beams Generated by Structured Laser-Irradiated Targets and its Application to Two-Photon Pair Production, Phys. Rev. Applied **13**, 054024 (2020).

[31] A. Golub, S. Villalba-Chávez, H. Ruhl, and C. Müller, Linear Breit-Wheeler pair production by high-energy

bremsstrahlung photons colliding with an intense X-ray laser pulse, Phys. Rev. D **103**, 016009 (2021).
[32] L. Esnault, E. d'Humières, A. Arefiev, and X. Ribeyre, Electron-positron pair production in the collision of real photon beams with wide energy distributions, Plasma Phys. Control. Fusion **63**, 125015 (2021).
[33] B. Kettle, D. Hollatz, E. Gerstmayr, G. M. Samarin, A. Alejo, S. Astbury, C. D. Baird, S. Bohlen, M. Campbell, C. Colgan *et al.*, A laser-plasma platform for photon-photon physics: The two photon Breit-Wheeler process, New J. Phys. **23**, 115006 (2021).
[34] Y. He, T. G. Blackburn, T. Toncian, and A. V. Arefiev, Dominance of gamma-gamma electron-positron pair creation in a plasma driven by high-intensity lasers, Commun. Phys. **4**, 139 (2021).
[35] Y. He, I. L. Yeh, T. G. Blackburn, and A. Arefiev, A single-laser scheme for observation of linear Breit-Wheeler electron-positron pair creation, New J. Phys. **23**, 115005 (2021).
[36] A. Golub, R. Egger, C. Müller, and S. Villalba-Chávez, Dimensionality-Driven Photoproduction of Massive Dirac Pairs Near Threshold in Gapped Graphene Monolayers, Phys. Rev. Lett. **124**, 110403 (2020).
[37] V. Yakimenko and I. V. Pogorelsky, Polarized γ source based on compton backscattering in a laser cavity, Phys. Rev. ST Accel. Beams **9**, 091001 (2006).
[38] T. Omori, M. Fukuda, T. Hirose, Y. Kurihara, R. Kuroda, M. Nomura, A. Ohashi, T. Okugi, K. Sakaue, T. Saito, J. Urakawa, M. Washio, and I. Yamazaki, Efficient Propagation of Polarization from Laser Photons to Positrons through Compton Scattering and Electron-Positron Pair Creation, Phys. Rev. Lett. **96**, 114801 (2006).
[39] G. Alexander *et al.*, Observation of Polarized Positrons from an Undulator-Based Source, Phys. Rev. Lett. **100**, 210801 (2008).
[40] D. Abbott, P. Adderley, A. Adeyemi, P. Aguilera, M. Ali, H. Areti, M. Baylac, J. Benesch, G. Bosson, B. Cade *et al.*, Production of Highly Polarized Positrons using Polarized Electrons at MeV Energies, Phys. Rev. Lett. **116**, 214801 (2016).
[41] J. Yan, J. M. Mueller, M. W. Ahmed, H. Hao, S. Huang, J. Li, V. N. Litvinenko, P. Liu, S. F. Mikhailov, V. G. Popov *et al.*, Precision control of gamma-ray polarization using a crossed helical undulator free-electron laser, Nat. Photonics **13**, 629 (2019).
[42] Y. F. Li, R. Shaisultanov, Y. Y. Chen, F. Wan, K. Z. Hatsagortsyan, C. H. Keitel, and J. X. Li, Polarized Ultrashort Brilliant Multi-GeV γ rays via Single-Shot Laser-Electron Interaction, Phys. Rev. Lett. **124**, 014801 (2020).
[43] A. G. Baier and V. N. Grozin, Complete analysis of polarization effects in $\gamma\gamma \to e^+e^-$ with REDUCE, arXiv:hep-ph/0209361.
[44] V. B. Berestetskii, E. M. Lifshitz, and L. P. Pitaevskii, *Quantum Electrodynamics* (Butterworth-Heinemann, London, 1982), Vol. 4.
[45] S. I. Kotkin, G. L. Polityko, and V. G. Serbo, Polarization of final electrons in the compton effect, Nucl. Instrum. Methods Phys. Res., Sect. A **405**, 30 (1998).
[46] A. G. Grozin, Complete analysis of polarization effects in $e\gamma \to e\gamma$ with REDUCE, arXiv:hep-ph/0209360.
[47] D. Y. Ivanov, G. L. Kotkin, and V. G. Serbo, Complete description of polarization effects in emission of a photon by an electron in the field of a strong laser wave, Eur. Phys. J. C **36**, 127 (2004).
[48] D. Y. Ivanov, G. L. Kotkin, and V. G. Serbo, Complete description of polarization effects in e^+e^- pair productionby a photon in the field of a strong laser wave, Eur. Phys. J. C **40** (2005).
[49] Supplemental Material http://link.aps.org/supplemental/10.1103/PhysRevD.105.L071902 mainly include the calculation of polarized LBW cross-section, the prescription of photon Stokes parameters and pair spin vectors, and the additional simulation results for polarized LBW pair production.
[50] F. Del Gaudio, T. Grismayer, R. A. Fonseca, and L. O. Silva, Compton scattering in particle-in-cell codes, J. Plasma Phys. **86**, 905860516 (2020).
[51] M. Schlickeiser and R. Bottcher, The pair production spectrum from photon-photon annihilation, Astron. Astrophys. **325**, 866 (1997).
[52] X. Ribeyre, E. d'Humières, O. Jansen, S. Jequier, and V. T. Tikhonchuk, Electron-positron pairs beaming in the Breit-Wheeler process, Plasma Phys. Control. Fusion **59**, 014024 (2017).
[53] X. Ribeyre, E. d'Humières, S. Jequier, and V. T. Tikhonchuk, Effect of differential cross section in Breit-Wheeler pair production, Plasma Phys. Control. Fusion **60**, 104001 (2018).
[54] H. A. Tolhoek, Electron polarization, theory and experiment, Rev. Mod. Phys. **28**, 277 (1956).
[55] K.-i. Hikasa, Transverse-polarization effects in e^+e^- collisions: The role of chiral symmetry, Phys. Rev. D **33**, 3203 (1986).
[56] F. Albert, S. G. Anderson, D. J. Gibson, C. A. Hagmann, M. S. Johnson, M. Messerly, V. Semenov, M. Y. Shverdin, B. Rusnak, A. M. Tremaine, F. V. Hartemann, C. W. Siders, D. P. McNabb, and C. P. J. Barty, Characterization and applications of a tunable, laser-based, MeV-class compton-scattering γ-ray source, Phys. Rev. ST Accel. Beams **13**, 070704 (2010).
[57] V. Tioukine, K. Aulenbacher, and E. Riehn, A mott polarimeter operating at MeV electron beam energies, Rev. Sci. Instrum. **82**, 033303 (2011).
[58] K. Aulenbacher, E. Chudakov, D. Gaskell, J. Grames, and K. D. Paschke, Precision electron beam polarimetry for next generation nuclear physics experiments, Int. J. Mod. Phys. E **27**, 1830004 (2018).
[59] J. M. Grames, C. K. Sinclair, M. Poelker, X. Roca-Maza, M. L. Stutzman, R. Suleiman, M. A. Mamun, M. McHugh, D. Moser, J. Hansknecht, B. Moffit, and T. J. Gay, High precision 5 MeV Mott polarimeter, Phys. Rev. C **102**, 015501 (2020).
[60] J. Granot, J. Cohen-Tanugi, and E. d. C. e Silva, Opacity buildup in impulsive relativistic sources, Astrophys. J. **677**, 92 (2008).
[61] D. Guetta, E. Pian, and E. Waxman, FERMI constraints on the high energy, ∼1 GeV, emission of long gamma ray bursts, Astron. Astrophys. **525**, A53 (2011).
[62] J. Poutanen and B. Stern, GeV breaks in blazars as a result of gamma-ray absorption within the broad-line region, Astrophys. J. Lett. **717**, L118 (2010).

[63] Y. S. Huang, Quantum-electrodynamical birefringence vanishing in a thermal relativistic pair plasma, Sci. Rep. **5**, 15866 (2015).

[64] G. Voisin, F. Mottez, and S. Bonazzola, Electron–positron pair production by gamma-rays in an anisotropic flux of soft photons, and application to pulsar polar caps, Mon. Not. R. Astron. Soc. **474**, 1436 (2018).

[65] R. Xue, R. Y. Liu, X. Y. Wang, H. Yan, and M. Böttcher, On the minimum jet power of TeV BL lac objects in the p–γ model, Astrophys. J. **871**, 81 (2019).